4-30-2007

Simulation of Interfacial Phonon Transport in Si–Ge Heterostructures Using an Atomistic Green's Function Method

W Zhang
Purdue University, zhang70@purdue.edu

Timothy Fisher
Birck Nanotechnology Center, School of Mechanical Engineering, Purdue University, tsfisher@purdue.edu

N. Mingo
NASA-Ames Center for Nanotechnology

Simulation of Interfacial Phonon Transport in Si–Ge Heterostructures Using an Atomistic Green's Function Method

W. Zhang

T. S. Fisher
e-mail: tsfisher@purdue.edu

School of Mechanical Engineering,
Birck Nanotechnology Center,
Purdue University,
West Lafayette, IN 47907

N. Mingo
NASA-Ames Center for Nanotechnology,
229-1,
Moffett Field, CA 94035

An atomistic Green's function method is developed to simulate phonon transport across a strained germanium (or silicon) thin film between two semi-infinite silicon (or germanium) contacts. A plane-wave formulation is employed to handle the translational symmetry in directions parallel to the interfaces. The phonon transmission function and thermal conductance across the thin film are evaluated for various atomic configurations. The contributions from lattice straining and material heterogeneity are evaluated separately, and their relative magnitudes are characterized. The dependence of thermal conductance on film thickness is also calculated, verifying that the thermal conductance reaches an asymptotic value for very thick films. The thermal boundary resistance of a single Si/Ge *interface is computed and agrees well with analytical model predictions. Multiple-interface effects on thermal resistance are investigated, and the results indicate that the first few interfaces have the most significant effect on the overall thermal resistance.* [DOI: 10.1115/1.2709656]

Introduction

The characteristic feature sizes of modern electronic devices are rapidly approaching nanometer scales, and nanoengineered materials such as superlattices and quantum wires have been shown to possess excellent thermoelectric properties [1]. Heat transport in these systems, particularly across embedded interfaces, is critical to their performance and can exhibit significant differences as compared to conventional Fourier heat conduction. In this paper, an atomistic Green's function method is developed to study cross-plane heat conductance through a strained thin film between two semi-infinite contacts and the thermal boundary resistance between two dissimilar diamond-structure crystals.

The atomistic Green's function method is an effective tool to simulate ballistic transport in nanoscale devices and has been widely used in the simulation of electron transport [2]. The primary advantage of this approach is its efficiency in handling interfacial and boundary scattering, two important mechanisms in nanoscale devices. The dominant phonon mean free path (MFP) in silicon at room temperature is approximately 300 nm [3]. When the device characteristic length is much smaller than the MFP, ballistic transport dominates, and the major resistance to heat flow is imposed by interfaces and boundaries.

Several theoretical models exist to estimate thermal boundary resistance (TBR). The acoustic mismatch model (AMM) by [4] accounts for long-wavelength phonons and relates the transmission coefficient to acoustic impedances of the two adjacent materials; therefore it is strictly valid only at low temperatures. The diffuse mismatch model (DMM) by [5] assumes complete diffuse scattering of phonons at interfaces and ascribes the thermal interface resistance to mismatches of phonon density of states. In order to estimate thermal boundary resistance with the DMM, the phonon density of states must be supplied, either from a priori calculations or experiments. Neither the AMM nor DMM includes the details of interfacial microstructure, i.e., in both models, thermal boundary resistance is determined solely by the two joining materials without regard to how they are joined. This approximation limits the application of these two models [6].

Several numerical tools have been employed to simulate subcontinuum heat conduction. One of them is based on the phonon Boltzmann transport equation (BTE), which describes phonon transport by a statistical distribution function. The BTE can be solved by making an analogy to the equation of radiative transport (ERT) [7], using finite volume methods [8] or with Monte Carlo methods [9], with various assumptions and simplifications. Yazdani and Asheghi [10] used the acoustic mismatch model to predict interface resistance between strained Si/SiGe and solved the BTE for phonons with a single mode relaxation time assumption in a strained silicon transistor. Prasher and Phelan [7] developed a scattering-mediated AMM with the BTE to investigate bulk scattering effects on thermal boundary resistance. In both studies, the phonon density of states and group velocity were supplied as assumed quantities, and different polarization branches needed to be considered separately. Further, the nature of phonon interfacial transport was simplified through AMM, DMM, or other models.

Another relevant computational tool is molecular dynamics (MD), which is computationally expensive and treats atomic vibrational modes classically. Thus, strictly speaking, it is not applicable at temperatures much lower than the Debye temperature. Picu et al. [11] employed equilibrium molecular dynamics to study strain and size effects in solid Ar nanostructures and concluded that lattice thermal conductivity in strained nanostructures under plane stress is controlled by boundary scattering. Abramson et al. [12] used nonequilibrium molecular dynamics to study interface and strain effects in Kr and Ar heterostructures and observed that an imposed tensile strain resulted in a significant decrease in thermal conductivity. Schelling et al. [13] used MD to simulate phonon wave-packet dynamics through perfectly coher-

Contributed by the Heat Transfer Division of ASME for publication in JOURNAL OF HEAT TRANSFER. Manuscript received December 15, 2005; final manuscript received May 30, 2006. Review conducted by Yogendra Joshi. Paper presented at the 2005 ASME International Mechanical Engineering Congress (IMECE2005), Orlando, FL, USA, November 5–11, 2005.

ent interfaces between two materials with different masses and obtained energy transmission coefficients that were similar to those of Young and Maris [14].

The atomistic Green's function method is based on a quantum mechanical description of the phonon energy distribution, rather than the classical description employed in MD. Therefore, the atomistic Green's function method has significant advantages over MD at low temperatures. As long as the harmonic assumption is satisfied, the atomistic Green's function (AGF) method retains these advantages over MD. Practical examples include nanostructures with characteristic lengths that are much smaller than phonon mean free paths (typically 100–300 nm at room temperature) and transport across interfaces. Computationally, the calculation of interfacial phonon transmission using Green's functions is much faster than that by MD. Many numerical challenges such as finite-size effects in MD are also mitigated.

Unlike the BTE with a boundary scattering model or a continuous acoustic wave model [15], atomistic numerical methods (including MD, lattice dynamics, and the atomistic Green's function method) provide sound solutions without excessively complicated appreciation of phonon transport fundamentals [16]. To date, atom-based simulations of phonon interfacial transport have not been widely investigated and documented. Young and Maris [14] investigated phonon transmission between two identical semi-infinite (face centered cubic) (FCC) lattices with different masses and spring constants using lattice dynamics, and the spectral dependence of the phonon transmission coefficient was calculated. Their method was later extended by Pettersson and Mahan [17] to handle dissimilar lattices. However, this method requires two lattices fully connected at the interface, whereas the atomistic Green's function method can be used in cases where the two materials are connected by a nonperiodic junction, such as a point contact or a nanowire. Sui Herman [18] used a modified Keating/valence-force-field model to study the effect of strain on phonon dispersion and elastic constants of Group IV semiconductors, but thermal transport calculations were not reported.

The atomistic Green's function method, as shown in this paper, provides an accurate and versatile approach to perform nanoscale heat transport simulations. The atomistic Green's function method is based on a dynamical equation and the quantum mechanical phonon energy distribution. The method incorporates the phonon density of states into transmission function calculations. Therefore no a priori knowledge of phonon density of states is required. The inputs are equilibrium locations of atoms and interatomic potentials, and experimentally fitted phonon dispersion curves are not needed. Under harmonic transport, the transmission function and thermal conductance given by the atomistic Green's function method are exact. The wave nature of phonon transport is also captured, and a method to introduce the effect of anharmonicity has recently been developed [19]. The atomistic Green's function method also holds the promise to provide boundary conditions for mesoscale simulation tools, such as BTE solvers.

Strained silicon technology provides a means to increase carrier mobility in the channel region of a metal–oxide–semiconductor field effect transistor (MOSFET) by altering electron energy bands to reduce effective mass and intervalley scattering rates. MOSFETs based on this technology exhibit 10–25% improvements in device performance metrics as compared to conventional unstrained silicon transistors [20]. Pop et al. [21] used a Monte Carlo method to simulate electron–phonon interactions in order to determine the phonon generation rate and associated Joule heating effects in bulk and strained silicon. They found that generated phonon distributions are different in bulk and strained silicon at low fields. Phonon transport simulations with the atomistic Green's function method in this emerging technology can provide not only insights into heat transport through the strained silicon layer, but also a potentially common framework to simulate electron–phonon scattering and related local heat generation and dissipation processes when combined with electron transport solvers.

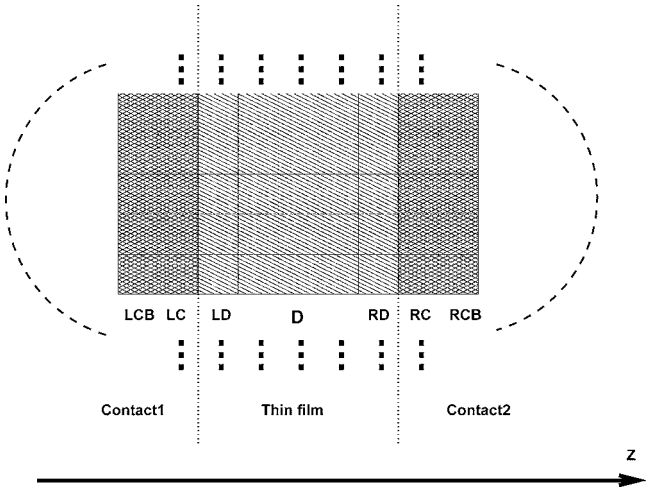

Fig. 1 Schematic diagram of a five-unit-cell thin film between two semi-infinite contacts. The definitions of different groups of atoms are shown. In this case, Region D includes three unit-cell layers.

The theoretical framework of the atomistic Green's function method in phonon transport simulations has been described previously and implemented for a nanowire system in Refs. [22,23]. The theory is extended in this paper to handle a thin-film system. The transmission function and thermal conductance (resistance) for strained thin films are evaluated, and their dependencies on thickness, temperature, and other factors are discussed. A special case is also considered in which the thermal boundary resistance between two dissimilar materials is predicted. The general AGF method presented in this paper can be readily extended to more complicated nanostructures (such as nanowires or nanocrystals with defects) between two bulk contacts.

Problem Definition

Actual atomic configurations at heterogeneous interfaces are very complicated and vary significantly with deposition conditions [24]. To define atomic locations in a reasonably simple way, an idealized geometry has been chosen and is shown in Fig. 1. The atomic lattice is based on an undistorted diamond lattice and is later modified using Poisson's ratio to reflect changes due to strain.

In Fig. 1, each square represents a unit cell in a crystal lattice. "Contact1" (including atom Groups LCB and LC) and "Contact2" (including atom Groups RCB and RC) are two semi-infinite thermal reservoirs at constant temperatures T_1 and T_2, respectively. Atom Group LC includes atoms in "Contact1" that bond with the thin-film atoms. Atoms in Group LCB do not have any bonds with the thin-film atoms. Therefore, the dynamical properties of these two regions (LCB and LC) are different. Similar definitions apply to atom groups RC and RCB. A thin film (including atom groups LD, D, and RD) of infinite extent in the x and y directions is placed between the two contacts. Atom Groups LD and RD include thin-film atoms that bond with "Contact1" and "Contact2" atoms, respectively. Atoms in Group D have no bond with either contact. In the cases discussed later, the contact and thin-film material can be either germanium or silicon, and their (100) directions are oriented along the z axis.

The size mismatch between silicon and germanium lattices creates either tensile or compressive strains on the thin film. The semi-infinite contacts are assumed to remain unstrained due to their bulk volumes. In this paper, we assume that the lattice mis-

Table 1 Computational parameters used in the construction of Si and Ge harmonic matrices. The first number in C_0 is the unstrained value and the second number is the strained value.

	Silicon	Germanium
Atomic mass m (kg)	4.664×10^{-26}	1.206×10^{-25}
Lattice constant (Å)	5.43	5.65
C_0 in Harrison's potential (eV)	49.1/44.8	47.2/51.2
C_1 in Harrison's potential (eV)	1.07	0.845
Poisson's ratio	0.28	0.26

match creates a pure-strained thin film without inducing dislocations. Such lattices typically occur in extremely thin films, while thicker films usually include buffer zones and relaxed lattices [25]. In the Ge/Si/Ge case (Ge contacts, Si thin film), germanium contacts stretch the silicon thin film by 4% in the in-plane direction (xy plane), creating biaxial strains of 0.04 in both x and y directions. The silicon thin-film lattice tends to maintain its volume, and consequently, it contracts in the z direction. We assume that the z strain can be calculated using the bulk Poisson's ratio (0.28 for silicon (100) and 0.26 for germanium (100) [26]). Thus, the z distance between any two atoms is reduced by a factor of approximately 0.01 (biaxial strain multiplied by Poisson's ratio). Similar lattice adjustments have been applied to the Si/Ge/Si case.

Theory

Harmonic Matrix and Interatomic Potential. The atomistic Green's function method starts by building harmonic matrices. Prior work [22] has shown that anharmonic scattering in Si at room temperature can be neglected if the device's characteristic length is less than 20 nm, and even at the 45 nm semiconductor technology node, many film structures possess cross-plane thicknesses less than 20 nm. In such cases, a harmonic potential can be used to build the harmonic matrix $\mathbf{H}$, which represents interactions among different degrees of freedom (d.o.f). The mathematical definition of the harmonic matrix is [22]

$$\mathbf{H} = \{H_{ij}\} = \frac{1}{\sqrt{M_i M_j}} \begin{cases} -\dfrac{\partial^2 U}{\partial u_i \partial u_j}, & \text{if } i \neq j \\ -\displaystyle\sum_{r\neq j} \dfrac{\partial^2 U}{\partial u_i \partial u_j}, & \text{if } i = j \end{cases} \tag{1}$$

where u_i and u_j refer to any two atomic displacement degrees of freedom respectively; and U represents the total bonding energy. M_i and M_j are atomic masses associated with degrees of freedom u_i and u_j, respectively. The dynamical equation of the entire lattice can be written as

$$(\omega^2\mathbf{I} - \mathbf{H})\tilde{u} = 0 \tag{2}$$

where $\tilde{u}$ is a column vector of degrees of freedom. We use Harrison's interatomic potintial [27] to evaluate the harmonic matrix $\mathbf{H}$

$$\Delta U_i = \frac{1}{2} C_0 \frac{(d_i - d_{i,e})^2}{d_{i,e}^2} + \frac{1}{2} C_1 (\Delta\theta_i)^2 \tag{3}$$

where d_i represents the bond length; and $d_{i,e}$ represents the equilibrium bond length. $\Delta\theta_i$ is the change to the equilibrium tetrahedral angle θ_i (1.9106 rad). Although this simple potential model has only two independent parameters, C_0 and C_1 (see potential parameters in Table 1), it includes bond-stretching/bending potentials and reproduces bulk phonon dispersion curves reasonably well [27]. This potential model was used to predict the thermal conductivity of silicon nanowires, and the numerical results agree well with experimental data [28]. Because of the harmonic assumption, potential variations in the vicinity of the equilibrium atomic positions are the only information needed to evaluate harmonic matrices. Near the equilibrium locations, more complicated inter-atomic potentials can be simplified parabolically to a form that is consistent with Harrison's potential. However, we also note that the bond-stretching and bond-bending parts of the potential are actually correlated, and other advanced potentials have been developed to address this problem [29].

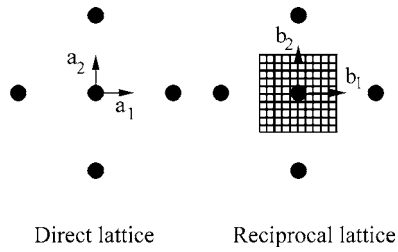

Fig. 2 The 2D direct lattice (left) and reciprocal lattice (right) in a fcc structure. A 10×10 mesh is placed on the first Brillouin zone in the right subfigure.

Plane-Wave Formulation in Thin Films. The system of interest in this work is infinitely large in the x and y directions and contains infinite degrees of freedom. Therefore the harmonic matrix defined in Eq. (1) is infinitely large. For these directions we use the wave vector representation, in terms of $\vec{\mathbf{k}}_\parallel$, to build harmonic matrices ($\tilde{\mathbf{H}}$) with the assumption of ideal translational invariance in x and y directions. The thin film and contacts are divided into unit-cell layers along the z axis. One unit cell in each layer is sufficient to represent the whole layer. A 6×6 harmonic matrix $\tilde{\mathbf{H}}_p$ is defined to represent the intralayer interaction in layer p, while another 6×6 harmonic matrix $\tilde{\mathbf{T}}_{p,q}$ is defined to represent the interlayer interaction between layer p and the layer to its right (q)

$$\tilde{\mathbf{H}}_p(\vec{\mathbf{k}}_\parallel) = \sum_{n=0}^{4} \mathbf{H}_{t,n} e^{-i\vec{\mathbf{k}}_\parallel \vec{\mathbf{R}}_n} \tag{4}$$

$$\tilde{\mathbf{T}}_{p,q}(\vec{\mathbf{k}}_\parallel) = \sum_{m=1}^{4} \mathbf{H}_{t,m} e^{-i\vec{\mathbf{k}}_\parallel \vec{\mathbf{R}}_m} \tag{5}$$

where t is an arbitrary unit cell on layer p. The index n loops through the neighboring unit cells of unit cell t that are in the same layer (p), including itself (n ranges from 0 to 4 for a (100) diamond lattice), and the index m loops through the neighboring cells in the next layer q (m ranges from 1 to 4 for a (100) diamond lattice). $\mathbf{H}_{t,n}$ (or $\mathbf{H}_{t,m}$) is the regular harmonic matrix that links unit cells t and n (or m). With these two types of matrices ($\tilde{\mathbf{H}}_p$ and $\tilde{\mathbf{T}}_{p,q}$), the complete harmonic matrix for any system can be assembled. For example, the matrix to represent an l-layer thin film is

$$\tilde{\mathbf{H}}_{\text{tf}}(\vec{\mathbf{k}}_\parallel) = \begin{bmatrix} \tilde{\mathbf{H}}_1 & \tilde{\mathbf{T}}_{1,2} & 0 & \cdots & 0 \\ \tilde{\mathbf{T}}_{2,1} & \tilde{\mathbf{H}}_2 & \tilde{\mathbf{T}}_{2,3} & \cdots & 0 \\ \vdots & \vdots & \vdots & \vdots & \vdots \\ 0 & \cdots & 0 & \tilde{\mathbf{T}}_{l,l-1} & \tilde{\mathbf{H}}_l \end{bmatrix} \tag{6}$$

where $\tilde{\mathbf{T}}_{p,q} = \tilde{\mathbf{T}}_{q,p}^{\dagger}$ (conjugate transpose). $\vec{\mathbf{k}}_\parallel$ in Eqs. (4)–(6) is an arbitrary two-dimensional (2D) lattice wave vector. Each wavevector ($\vec{\mathbf{k}}_\parallel = k_x\vec{b}_1 + k_y\vec{b}_2$) represents phonons traveling in one distinct x-y direction. The 2D lattice perpendicular to the (100) direction is a square lattice, and its first Brillouin zone is a square ($k_x \in [-\sqrt{2}\pi/a, \sqrt{2}\pi/a), k_y \in [-\sqrt{2}\pi/a, \sqrt{2}\pi/a)$), as shown in Fig. 2. Because of translational invariance in the x and y directions, the

transmission function for each $\vec{\mathbf{k}}_\parallel$ can be solved independently, and the total heat flux can be expressed as an integral of the independent heat fluxes for each $\vec{\mathbf{k}}_\parallel$. We emphasize that this simplification would not be valid if the x and y translational symmetries were broken, such as in the case of a point contact. The total heat flux calculation must account for phonons traveling in all directions. Thus, it is expressed as an integral over $\vec{\mathbf{k}}_\parallel$ as shown in the next section.

Green's Function Matrices. The response of a dynamic system (defined by Eq. (2)) to an infinitesimal perturbation can be described by a Green's function. In the present work, the Green's functions $\mathbf{g}_{\mathrm{LCB}}$ and $\mathbf{g}_{\mathrm{RCB}}$ represent the responses of the two semi-infinite contacts, respectively

$$\mathbf{g}_{\mathrm{LCB}}(\omega,\vec{\mathbf{k}}_\parallel) \equiv \lim_{\delta\to 0}[(\omega^2+\delta i)\mathbf{I}-\widetilde{\mathbf{H}}_{\mathrm{LCB}}(\vec{\mathbf{k}}_\parallel)]^{-1} \tag{7}$$

$$\mathbf{g}_{\mathrm{RCB}}(\omega,\vec{\mathbf{k}}_\parallel) \equiv \lim_{\delta\to 0}[(\omega^2+\delta i)\mathbf{I}-\widetilde{\mathbf{H}}_{\mathrm{RCB}}(\vec{\mathbf{k}}_\parallel)]^{-1} \tag{8}$$

where $\mathbf{H}_{\mathrm{LCB}}$ and $\mathbf{H}_{\mathrm{RCB}}$ are the dynamical matrices of the left and right contacts. $\mathbf{g}_{\mathrm{LCB}}$ and $\mathbf{g}_{\mathrm{RCB}}$ are determined by decimation techniques [30,31], and their imaginary parts are directly associated with phonon density of states [32]. In Eqs. (7) and (8), δ is a small number corresponding to phonon energy dissipation in contacts whose role is elaborated in Ref. [33]. The choice of δ affects the energy resolution of the uncoupled Green's function and subsequent calculations. A smaller δ value gives better energy resolution but requires longer computational times. A method to choose an appropriate value of the perturbation δ is documented in Ref. [22].

Referring again to Fig. 1, atoms in LC (or RC) are different than other atoms in "Contact1" (or "Contact2") because they are bonded to atoms in the thin film. Therefore, $\mathbf{g}_{\mathrm{LC}}$ ($\mathbf{g}_{\mathrm{RC}}$) must be defined separately and differs from $\mathbf{g}_{\mathrm{LCB}}$ ($\mathbf{g}_{\mathrm{RCB}}$) in a general heterogeneous system. Green's function matrices $\mathbf{g}_{\mathrm{LC}}$ and $\mathbf{g}_{\mathrm{RC}}$ are defined as

$$\mathbf{g}_{\mathrm{LC}}(\omega,\vec{\mathbf{k}}_\parallel) \equiv [\omega^2\mathbf{I}-\widetilde{\mathbf{H}}_{\mathrm{LC}}(\vec{\mathbf{k}}_\parallel)-\widetilde{\mathbf{T}}_{\mathrm{LC,LCB}}\mathbf{g}_{\mathrm{LCB}}\widetilde{\mathbf{T}}_{\mathrm{LCB,LC}}]^{-1} \tag{9}$$

$$\mathbf{g}_{\mathrm{RC}}(\omega,\vec{\mathbf{k}}_\parallel) \equiv [\omega^2\mathbf{I}-\widetilde{\mathbf{H}}_{\mathrm{RC}}(\vec{\mathbf{k}}_\parallel)-\widetilde{\mathbf{T}}_{\mathrm{RC,RCB}}\mathbf{g}_{\mathrm{RCB}}\widetilde{\mathbf{T}}_{\mathrm{RCB,RC}}]^{-1} \tag{10}$$

where $\widetilde{\mathbf{H}}_{\mathrm{LC}}$ and $\widetilde{\mathbf{H}}_{\mathrm{RC}}$ are intralayer matrices (see Eq. (4)) for regions LC and RC, respectively.

The Green's function of the device is defined as

$$\mathbf{G}(\omega,\vec{\mathbf{k}}_\parallel) \equiv [\omega^2\mathbf{I}-\widetilde{\mathbf{H}}_{\mathrm{tf}}-\mathbf{\Sigma}_L-\mathbf{\Sigma}_R]^{-1} = \begin{bmatrix} \mathbf{G}_{\mathrm{LD,LD}} & \mathbf{G}_{\mathrm{LD,D}} & \mathbf{G}_{\mathrm{LD,RD}} \\ \mathbf{G}_{\mathrm{D,LD}} & \mathbf{G}_{\mathrm{D,D}} & \mathbf{G}_{\mathrm{D,RD}} \\ \mathbf{G}_{\mathrm{RD,LD}} & \mathbf{G}_{\mathrm{RD,D}} & \mathbf{G}_{\mathrm{RD,RD}} \end{bmatrix} \tag{11}$$

where $\widetilde{\mathbf{H}}_{\mathrm{tf}}$ is the harmonic matrix of the thin film (see Eq. (6)). $\mathbf{\Sigma}_L$ and $\mathbf{\Sigma}_R$ are self-energy matrices that physically represent changes to the thin film's dynamical behavior caused by contacts

$$\mathbf{\Sigma}_L(\omega,\vec{\mathbf{k}}_\parallel) \equiv \begin{bmatrix} \tau_L & 0 & 0 \\ 0 & 0 & 0 \\ 0 & 0 & 0 \end{bmatrix} \tag{12}$$

$$\mathbf{\Sigma}_R(\omega,\vec{\mathbf{k}}_\parallel) \equiv \begin{bmatrix} 0 & 0 & 0 \\ 0 & 0 & 0 \\ 0 & 0 & \tau_R \end{bmatrix} \tag{13}$$

τ_L and τ_R are defined as

$$\tau_L(\omega,\vec{\mathbf{k}}_\parallel) \equiv \widetilde{\mathbf{T}}_{\mathrm{LD,LC}}\mathbf{g}_{\mathrm{LC}}\widetilde{\mathbf{T}}_{\mathrm{LC,LD}} \tag{14}$$

$$\tau_R(\omega,\vec{\mathbf{k}}_\parallel) \equiv \widetilde{\mathbf{T}}_{\mathrm{RD,RC}}\mathbf{g}_{\mathrm{RC}}\widetilde{\mathbf{T}}_{\mathrm{RC,RD}} \tag{15}$$

where $\widetilde{\mathbf{T}}_{\mathrm{LD,LC}}$, $\widetilde{\mathbf{T}}_{\mathrm{LC,LD}}$, $\widetilde{\mathbf{T}}_{\mathrm{RD,RC}}$, and $\widetilde{\mathbf{T}}_{\mathrm{RC,RD}}$ are matrices that link contact and thin-film atom groups (see Eq. (5)). Matrices $\mathbf{\Gamma}_L$ and $\mathbf{\Gamma}_R$, later used in the expression of the transmission function, are defined as

$$\mathbf{\Gamma}_L(\omega,\vec{\mathbf{k}}_\parallel) \equiv i(\tau_L-\tau_L^\dagger) \tag{16}$$

$$\mathbf{\Gamma}_R(\omega,\vec{\mathbf{k}}_\parallel) \equiv i(\tau_R-\tau_R^\dagger) \tag{17}$$

and i is the unitary imaginary number.

Transmission and Heat Flux. Our ultimate goal is to calculate the heat flum and thermal conductance across thin films. The propagation of phonons between two contacts is determined by the transmission function $\Xi\ (\omega,\vec{\mathbf{k}}_\parallel)$ [34]

$$\Xi(\omega,\vec{\mathbf{k}}_\parallel) = \mathrm{Trace}[\mathbf{\Gamma}_L\mathbf{G}_{\mathrm{LD,RD}}\mathbf{\Gamma}_R\mathbf{G}_{\mathrm{LD,RD}}^\dagger] \tag{18}$$

$\mathbf{G}_{\mathrm{LD,RD}}$ in Eq. (18) is the top right block matrix in the device Green's function matrix (see Eq. (11)). The total heat flux is defined as an integral over frequency and $\vec{\mathbf{k}}_\parallel$

$$J = \int_0^\infty \int_{\vec{\mathbf{k}}_\parallel} \frac{\hbar\omega}{2\pi}\Delta\widetilde{N}(\omega)\Xi(\omega,\vec{\mathbf{k}}_\parallel)\frac{d\vec{\mathbf{k}}_\parallel}{(2\pi)^2}d\omega \tag{19}$$

The integral over $\vec{\mathbf{k}}_\parallel$ in Eq. (19) can be converted to a summation over a finite number of $\vec{\mathbf{k}}_\parallel$ upon discretizing the first Brillouin zone (see Fig. 2) with an $N\times N$ uniform mesh

$$J = \frac{1}{s}\int_0^\infty \frac{\hbar\omega}{2\pi}\Delta\widetilde{N}\left[\frac{1}{N^2}\sum_{\vec{\mathbf{k}}_\parallel}\Xi(\omega,\vec{\mathbf{k}}_\parallel)\right]d\omega \tag{20}$$

where s is the cross-sectional area of one unit cell. If the temperature difference between the two bulk contacts is sufficiently small, the phonon occupation difference $\Delta\widetilde{N}(\omega)$ in Eq. (19) becomes

$$\Delta\widetilde{N}(\omega) = \frac{\hbar\omega}{k_B T^2}\frac{e^{\hbar\omega/k_B T}}{(e^{\hbar\omega/k_B T}-1)^2}\Delta T \tag{21}$$

Otherwise, actual occupation numbers can be used to calculate the phonon occupation difference ($\Delta\widetilde{N}=\widetilde{N}_{\mathrm{contact1}}-\widetilde{N}_{\mathrm{contact2}}$). The thermal conductance across a thin film is then defined as the ratio of heat flux to temperature difference

$$\sigma = \frac{J}{\Delta T}\left(\frac{\mathrm{W}}{\mathrm{m}^2\,\mathrm{K}}\right) \tag{22}$$

Thermal resistance (R) is the inverse of conductance and has units of [m^2 K/W].

Results and Discussion

The atomistic Green's function method described above has been used to simulate ballistic phonon transport in a thin-film system. Several numerical benchmarks, such as the known parabolic frequency dependence of a pure material's transmission function at low frequencies [28], were conducted before the following numerical investigations. The thermal conductance of a pure material has also been verified to exhibit a T^3 dependence at low temperatures. Upon testing for grid independence, a Brillouin-zone mesh of 100×100 was needed to achieve thermal conductances that converged to within 1%. The computational time varies from several minutes to several hours on a common workstation in the following cases.

The Effects of Heterogeneous Materials and Strains. In the Si/Ge/Si and Ge/Si/Ge heterogeneous thin-film cases, thermal resistance occurs due to two factors. One factor is the heterogeneous-material effect, which causes mismatches of phonon density of states and group velocity. Another factor is lattice

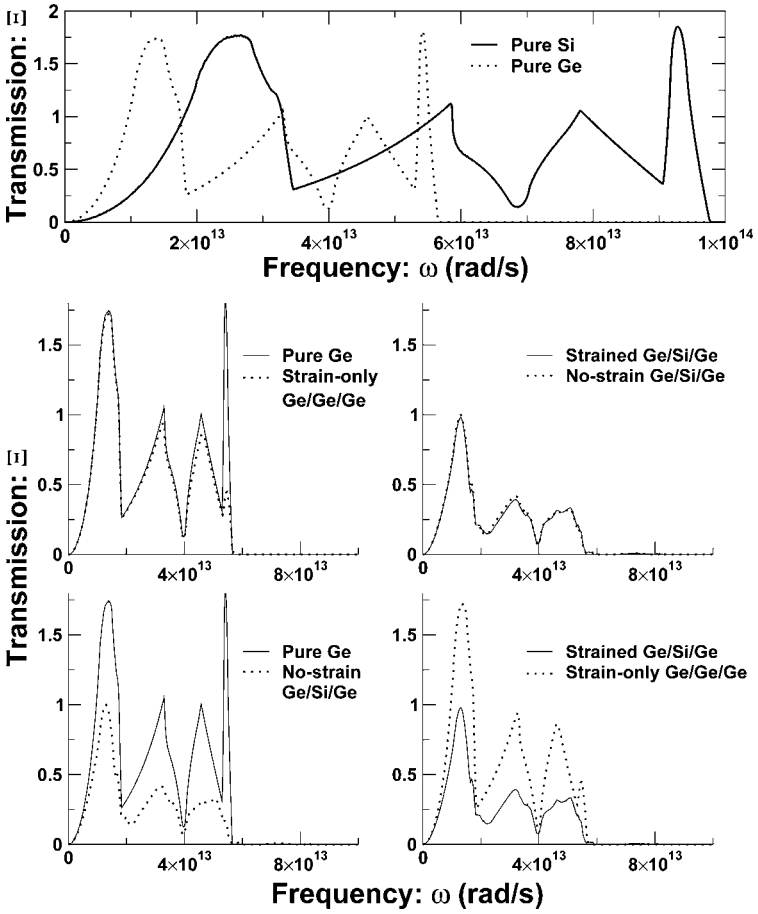

Fig. 3 Comparisons of full-spectrum transmission functions

strain, which displaces atoms and alters bond strength. Several computational examples are constructed here to demonstrate the relative significance of these two effects.

Transmission functions of these different atomic configurations are compared in Figs. 3 and 4. A strained heterogeneous case in which a stretched silicon thin film is placed between two germanium contacts (represented by "Strained Ge/Si/Ge") and another strained heterogeneous case in which a compressed germanium thin film is placed between two silicon contacts (represented by "Strained Si/Ge/Si") are included. Strains displace atoms away from their equilibrium positions. Therefore, both the geometric configuration of atoms (bond length and bond angles) and the force constants between atoms need to be modified. Based on Grüneisen's rule, we estimate that the change in the primary force constant (C_0 in Table 1) is four times that of the bond length.

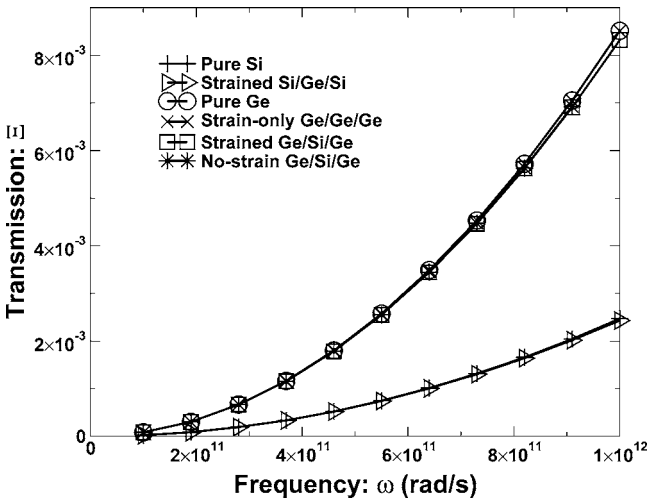

Fig. 4 Comparison of the straining effect with the heterogeneous-material effect on phonon transmission functions across a one-unit-cell thin film at low frequencies

The "No-strain Ge/Si/Ge" and "Strain-only Ge/Ge/Ge" cases shown in Figs. 3 and 4 are not physical but are included as informative thought experiments. The "No-strain Ge/Si/Ge" case is derived from the pure germanium case, in which germanium atoms in the thin-film region are replaced by silicon atoms while the lattice in the thin-film region remains a germanium lattice. In this case, only the heterogeneous effect exists because strain has been artificially removed. The "Strain-only Ge/Ge/Ge" case is derived from the "Strained Ge/Si/Ge" case such that silicon atoms in the thin-film region are replaced with germanium atoms, but the thin-film lattice remains stretched as in the "Strained Ge/Si/Ge" case. In this case, only lattice-straining effects exist because all atoms are germanium. In all cases discussed in this subsection, the film thickness equals the thickness of one unit cell in the (100) direction.

In pure materials, the phonon transmission function at one frequency depends only on the number of available phonon modes at that frequency. Pure germanium is known to have a higher density of states at low frequency than pure silicon [35]. Therefore, its transmission is higher than that of pure silicon at low frequencies. This trend is confirmed by predictions from the atomistic Green's function method, as shown by the pure Si and pure Ge results in Fig. 3(*a*). Pure silicon also has a more extensive spectrum than

Table 2 Zero-frequency group velocities of longitudinal acoustic (LA) phonons and transverse acoustic (TA) phonons calculated by Harrison's potential (the first number), compared with the zero-frequency group velocities estimated from elastic constants by Holland[a] (the second number). Harrison's potential is known to underestimate the zero-frequency group velocities. Densities of Si and Ge are shown as well. These values obtained from Harrison's potential are used in the acoustic mismatch model to predict the thermal boundary resistance across a Si/Ge interface.

	Silicon	Germanium
LA group velocity (m/s)	6877/8480	4114/4920
TA group velocity (m/s)	3535/5860	1978/3550
Density (kg/m^3)	2330	5323

[a]See Ref. [42].

pure germanium. The maximum phonon frequency is approximately 98×10^{12} rad/s in silicon and approximately 58×10^{12} rad/s in germanium.

The results of these calculations indicate that the straining effect is small in the ballistic transport regime in comparison to the heterogeneous-material effect. As shown in Fig. 3(*b*), no significant difference exists between the pure Ge and the strain-only Ge/Ge/Ge cases. If we compare the strained Ge/Si/Ge case to the no-strain Ge/Si/Ge case, the difference is also negligible. However, the difference between the pure Ge case and the no-strain Ge/Si/Ge case is large, as is the difference between the strained Ge/Si/Ge case and the strain-only Ge/Ge/Ge case (see Fig. 3(*b*)). The Si–Ge lattice mismatch is only 4%. The difference between silicon and germanium atomic masses is more than 50%, and the difference between their group velocities is approximately 40% (see Tables 1 and 2). This large difference in group velocities causes heterogeneous effects to be more prominent.

The transmission functions at low frequencies converge to two curves, corresponding to pure Si and pure Ge (see Fig. 4). We note that for the ultralow frequencies considered in Fig. 4 (for which the transmission function goes to zero), a much finer Brillouin zone mesh (3000×3000) was employed to produce the parabolic frequency dependence. The straining and heterogeneous-material effects both vanish because the lattice vibrates very slowly at low frequencies, and the whole solid resembles a rigid body, with neighboring atoms vibrating nearly in phase. Therefore, heterogeneous-material and straining effects are minor at low frequencies. This phenomenon also causes the low-temperature conductances to collapse to those of two pure materials, because low-frequency phonons dominate thermal transport at low temperatures. However, at room temperature, the heterogeneous interface effect is significant. The conductance of Ge/Si/Ge is approximately half that of pure Ge at room temperature, and the room-temperature conductance of Si/Ge/Si is 30% that of pure Si. At room temperature and higher, the conductance of Ge/Si/Ge is close to the conductance of Si/Ge/Si (see Fig. 5). This result is related to the fact that the areas under the Si/Ge/Si and Ge/Si/Ge transmission curves are comparable around the dominant phonon frequency at room temperature.

In the ballistic transport regime, scattering is only caused by interfaces and boundaries, and the scattering rate is roughly a constant that is independent of temperature. Therefore, thermal conductance is governed by the average phonon energy and has the same temperature dependence as thermal capacitance. Consequently, as shown in Fig. 5, thermal conductance increases with temperature and reaches a plateau at temperatures significantly higher than the Debye temperature.

Film Thickness Dependence. Figure 6 shows the thermal conductance through a Ge/Si/Ge system as a function of film thickness at different temperatures. The thickness of the thin film is

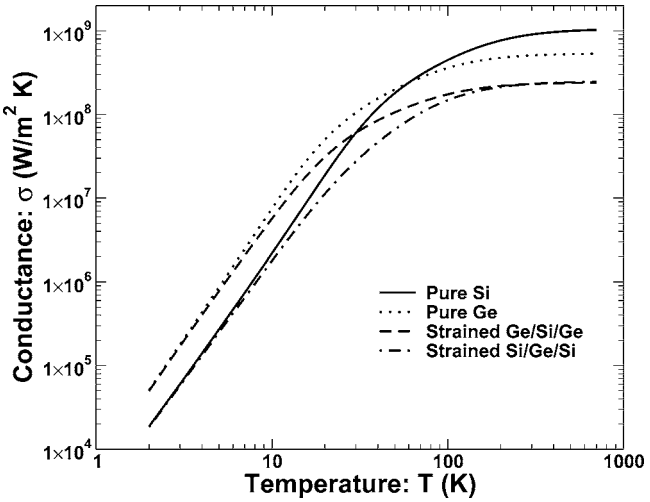

Fig. 5 Comparison of the thermal conductances of heterogeneous materials and those of homogeneous materials across a one-unit-cell thin film

expressed in terms of the number of unit cells. For a strained silicon thin film, one unit cell has a thickness of 2.69 Å. In the ballistic transport regime, the film thickness dependence of conductance is mainly attributed to the coupling and decoupling of phonon wave functions. If the two interfaces are extremely close, phonons can easily propagate from one side to another; thus the conductance in the one-unit-cell case is the largest. As the film thickness increases, thermal conductance decreases. Finally the conductance converges to the value corresponding to an infinitely thick, scattering-free film.

Thermal Boundary Resistance Across a Single Si/Ge Interface. TBR is present across interfaces between any dissimilar materials, and it results from differences in lattice vibration properties. If the material in the thin-film region is selected to be the same as that of one contact region, a single interface between the thin film and the other contact is created. Consequently, the atomistic Green's function method described above can be used to calculate TBR. However, the straining effect cannot be easily included in this structure because the three-dimensional layout of the interfacial atoms is complicated and difficult to predict. Thus, we choose to simulate the TBR between Si and Ge, assuming that

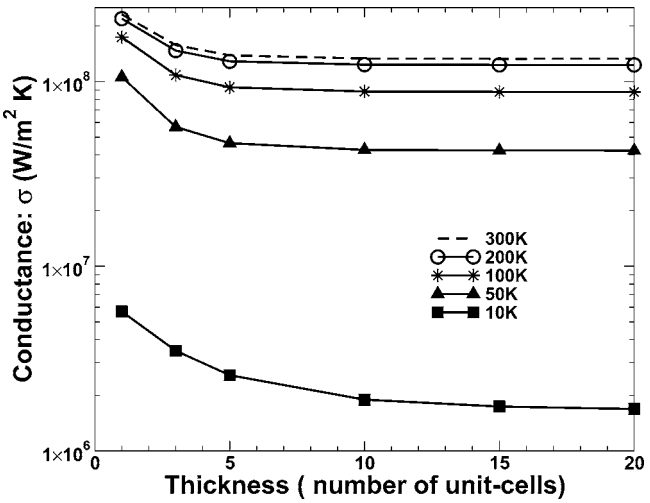

Fig. 6 Thickness dependence of thermal conductance in the Ge/Si/Ge configuration. Each unit cell is 2.69 Å.

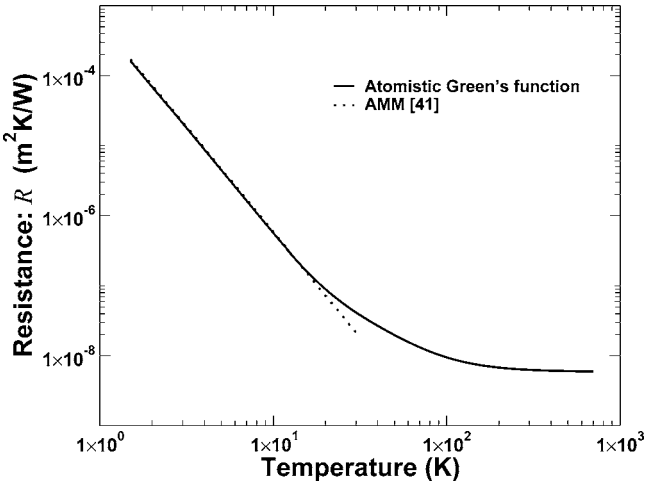

Fig. 7 Comparison of the thermal boundary resistance across a Si/Ge interface calculated by atomistic Green's function method to that by the acoustic mismatch model [41]

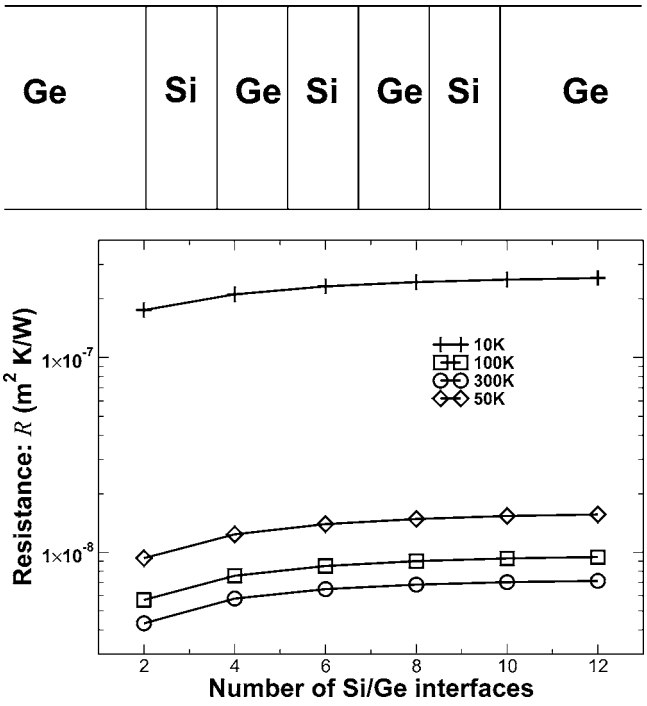

Fig. 8 The effect of multiple interfaces on thermal resistance

they both have germanium lattice distances.

Direct TBR measurements of Si/Ge interfaces are not readily available because most prior work [36,37], has reported only the thermal conductivity of Si/Ge superlattices. It remains unclear how to convert the thermal conductivity of a nanometer-size periodic structure to the thermal conductance of a single interface. In one attempt [38], the converted thermal interface conductance was reported to be ten times larger than the largest thermal interface conductance ever measured. Direct measurements of thermal resistance for other heterogeneous materials have been conducted by several groups. Stoner and Maris [39] used a picosecond optical technique to measure the thermal boundary resistances between metals and dielectrics. Costescu et al. [40] measured the TBR between epitaxial TiN and single crystal oxide with the time-domain thermoreflectance (TDTR) method.

The acoustic mismatch model (AMM) has been used to estimate the thermal conductance of a single interface. This model assumes that phonon interfacial transport is governed by continuum acoustics, and the interface is treated as an ideal plane. Therefore, it produces similar results at low temperatures to the atomistic Green's function method. We use the AMM thermal boundary resistance equation and associated tables published by Cheeke et al. [41] to estimate TBR at low temperatures ($T < 30$ K). Harrison's potential is used again to calculate bulk dispersion curves and group velocities in the (100) direction. The calculated zero-frequency group velocities, the zero-frequency group velocities estimated from elastic constants by Holland [42], and densities used in the AMM are listed in Table 2. Harrison's potential is known to predict lower group velocities [27].

A comparison between the atomistic Green's function results and the TBR predicted by the AMM is shown in Fig. 7. The AMM and the atomistic Green's function method both predict an expected cubic temperature dependence of TBR at low temperatures and agree very well at temperatures less than 20 K. This result is expected because the dominant phonons at low temperatures exhibit linear dispersion and the AMM works reasonably well. The Si/Ge interface produces a thermal boundary resistance of 6.2×10^{-9} m^2 K/W at room temperature according to the present results. The calculated interface thermal resistances can be used as boundary conditions in large-scale BTE simulations. In a rigorous BTE simulation that distinguishes phonon branch, phonon wave vector, and phonon frequency, the AGF method also must be (and can be) decomposed in terms of these variables.

Thermal Resistance Across Multiple Si/Ge Interfaces. Multiple-interface structures are of great importance in engineering applications. The overall thermal resistance of a multiple-interface structure is generally considered to increase with additional interfaces, because more phonons are reflected or scattered at interfaces. To evaluate the dependence of thermal resistance on the number of interfaces, the device region shown in Fig. 1 was made to include a multiple-interface structure. As an example, a six-interface structure is shown in Fig. 8(*a*). Mathematically, the matrix $\tilde{\mathbf{H}}_{\text{tf}}$ in Eq. (6) now is more complicated and contains contributions from each layer. Every layer in the multiple-interface structure is one-unit-cell thick. The effects of strain are excluded from the calculation because they were shown to be negligible in the foregoing analysis. Resistances at different temperatures as functions of the number of interfaces are shown in Fig. 8(*b*). The trend in the figure confirms that as the number of interfaces increases, thermal resistance increases. However, the change from two interfaces to four interfaces is much larger than changes caused by additional interfaces. The thermal resistance curve eventually levels out and approaches an asymptotic value. This observation agrees with a previous study [12], with the conclusion that the effect of the first few interfaces is much more significant than subsequently added interfaces.

To make a quantitative comparison between the AGF method and prior experimental data, we have simulated the superlattice sample with the shortest period (3 nm) considered in the experimental study of Lee et al. [38], and the results are shown in Fig. 9. The thermal conductance is plotted as a function of the total superlattice sample thickness for a temperature of 200 K. Because of the higher computational expense in simulating the full thickness (900 nm) due to the fine $\vec{\mathbf{k}}_{\parallel}$ discretization, we have calculated several cases of shorter samples. A clear conductance asymptote of 9.5×10^{7} W/m^2 K is reached beyond 20 nm and agrees with the trend shown in Fig. 8(*b*). The extrapolated thermal conductance at 900 nm is approximately one order of magnitude larger than the experimental thermal conductance. The difference can be ascribed to anharmonic effects in the experiment and to possible imperfections in the superlattice sample.

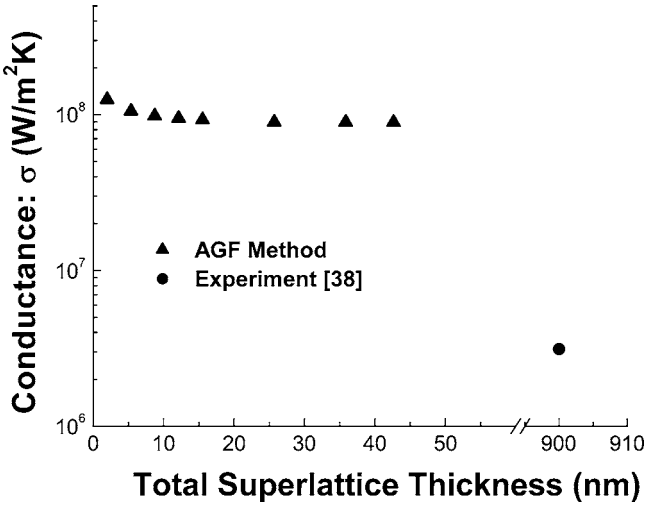

Fig. 9 Comparison of the thermal conductance of Si–Ge superlattice samples with 3 nm period at 200 K. The experimental result is from Lee et al. [38].

Conclusions

We have developed and described an atomistic Green's function method to study phonon transmission and thermal conductance (resistance) of atomistically defined Ge/Si/Ge and Si/Ge/Si strained thin films. The straining effect on thermal transport is found to be negligible as compared to the heterogeneous-material effect. At low frequencies, the transmission functions of the heterogeneous cases converge to those of the homogeneous cases because long phonon wavelengths result in rigid-body-like atomic motions. Room-temperature thermal conductances are reduced significantly by heterogeneous interfaces. The ballistic thermal conductance decreases as the thickness of the thin-film increases and reaches an asymptotic value, corresponding to the value of an infinitely thick film. We have also computed the thermal boundary resistance of a single Si/Ge interface and verified that it agrees with AMM results at low temperatures. A multiple interface case was also investigated, showing that the first few heterogeneous interfaces affect the thermal resistance to a much larger extent than subsequent interfaces.

Nomenclature

J = heat flux, W/m^2
M = atomic mass, kg
$\tilde{N}$ = phonon occupation number
N = mesh size, see Eq. (20)
R = thermal resistance, $m^2\,K/W$
T = temperature, K
U = interatomic potential, J
$\vec{\mathbf{k}}$ = wave vector, 1/m
a = lattice constant, m
i = unit of imaginary number
k_B = Boltzmann constant, $m^2\,kg/s^2\,K$
s = cross-sectional area, m^2
u = displacement degree of freedom, m
d = bond length, m

Greek Symbols

δ = A small number corresponding to phonon energy dissipation in contacts
$\hbar$ = Planck constant, $m^2\,kg/s$
ω = angular frequency, rad/s
σ = thermal conductance, $W/m^2\,K$
Ξ = Transmission function

Vector and Matrix

$\mathbf{\Gamma}$ = matrix defined in Eqs. (16) and (17)
$\mathbf{\Sigma}$ = self-energy matrix defined in Eqs. (12) and (13)
τ = matrix defined in Eqs. (14) and (15)
$\mathbf{G}$ = Green's function matrix defined in Eq. (11)
$\mathbf{g}$ = uncoupled Green's function matrix defined in Eqs. (9) and (10)
$\mathbf{H}$ = harmonic matrix, defined in Eq. (1)
$\mathbf{I}$ = unity matrix
$\tilde{\mathbf{H}}$ = matrix representing intralayer interaction, defined in Eq. (4)
$\tilde{\mathbf{T}}$ = matrix representing interlayer interaction, defined in Eq. (5)
$\tilde{u}$ = column vector consisting of vibrational degrees of freedom
$\vec{\mathbf{R}}$ = lattice vector

Subscripts and Superscripts

D = device region
LC = left contact region
LCB = left contact bulk region
LD = left device region
RC = right contact region
RCB = right contact bulk region
RD = right device region
tf = thin film
i = matrix row index, also the index of degree of freedom
j = matrix column index, also the index of degree of freedom
m = unit cell running index
n = unit cell running index
p = layer index
q = layer index
r = degree of freedom running index
t = unit cell index
$\dagger$ = conjugate transpose of a matrix
$\|$ = parallel direction to the thin film

References

[1] Chen, G., Dresselhaus, M., Dresselhaus, G., Fleurial, J., and Caillat, T., 2003, "Recent Developments in Thermoelectric Materials," Int. Mater. Rev., **48**(1), pp. 45–66.
[2] Datta, S., 2000, "Nanoscale Device Modeling: The Green's Function Method," Superlattices Microstruct., **28**, pp. 253–278.
[3] Ju, Y., and Goodson, K., 1999, "Phonon Scattering in Silicon Films With Thickness of Order 100 nm," Appl. Phys. Lett., **74**(20), pp. 3005–3007.
[4] Little, W., 1959, "The Transport of Heat Between Dissimilar Solids at Low Temperature," Can. J. Phys., **37**, pp. 334–349.
[5] Swartz, E., and Pohl, R., 1989, "Thermal Boundary Resistance," Rev. Mod. Phys., **61**, pp. 605–668.
[6] Stevens, R., Smith, A., and Norris, P., 2005, "Measurement of Thermal Boundary Conductance of a Series of Metal-Dielectric Interfaces by the Transient Thermoreflectance Technique," ASME J. Heat Transfer, **127**, pp. 315–322.
[7] Prasher, R., and Phelan, P., 2001, "A Scattering-Mediated Acoustic Mismatch Model for the Prediction of Thermal Boundary Resistance," ASME J. Heat Transfer, **123**, pp. 105–112.
[8] Narumanchi, S., Murthy, J., and Amon, C., 2004, "Submicron Heat Transport model in Silicon Accounting for Phonon Dispersion and Polarization," ASME J. Heat Transfer, **126**, pp. 946–955.
[9] Mazumdar, S., and Majumdar, A., 2001, "Monte Carlo Study of Phonon Transport in Solid Thin Films including Dispersion and Polarization," ASME J. Heat Transfer, **123**, pp. 749–759.
[10] Yazdani, K., and Asheghi, M., 2004, "Ballistic Phonon Transport in Strained Si/SiGe Nanostructures With an Application to Strained-silicon Transistors," *Proceedings of the 9th Intersociety Conference on Thermal and Thermomechanical Phenomena In Electronic Systems*, Las Vegas, NV, June 1–4, Paper No. 04CH37543.
[11] Picu, R., Borca-Tasciuc, T., and Pavel, M., 2003, "Strain and Size Effects on Heat Transport in Nanostructure," J. Appl. Phys., **93**(6), pp. 3535–3539.
[12] Abramson, A., Tien, C., and Majumdar, A., 2002, "Interface and Strain Effects on the Thermal Conductivity of Heterostructures: A Molecular Dynamics Study," ASME J. Heat Transfer, **124**(5), pp. 963–970.

[13] Schelling, P., Phillpot, S., and Keblinski, P., 2002, "Phonon Wave-Packet Dynamics at Semiconductor Interfaces by Molecular-Dynamics Simulation," Appl. Phys. Lett., **80**, pp. 2484–2486.
[14] Young, D., and Maris, H., 1989, "Lattice-dynamical Calculation of the Kapitza Resistance Between FCC Lattices," Phys. Rev. B, **40**(6), pp. 3685–3693.
[15] Nishiguchi, N., Tamura, S., and Nori, F., 1993, "Phonon-transmission Rate, Fluctuations, and Localization in Random Semiconductor Superlattices: Green's-Function Approach," Phys. Rev. B, **48**, pp. 2515–2528.
[16] Cahill, D., Ford, W., Goodson, K., Mahan, G., Majumdar, A., Maris, H., Merlin, R., and Phillpot, S., 2003, "Nanoscale Thermal Transport," J. Appl. Phys., **93**(2), pp. 793–818.
[17] Pettersson, S., and Mahan, G., 1990, "Theory of the Thermal Boundary Resistance Between Dissimilar Lattices," Phys. Rev. B, **42**, pp. 7386–7390.
[18] Sui, Z., and Herman, I., 1993, "Effect of Strain on Phonons in Si, Ge, and Si/Ge Heterostructures," Phys. Rev. B, **48**, pp. 17938–17953.
[19] Mingo, N., 2006, "Anharmonic Phonon Flow Through Molecular Sized Junctions," Phys. Rev. B, **74**, p. 125402.
[20] Thompson, S., Armstrong, M., Auth, C., Alavi, M., Buehler, M., Chau, R., Cea, S., Ghani, T., Glass, G., Hoffman, T., Jan, C., Kenyon, C., Klaus, J., Kuhn, K., Ma, Z., Mcintyre, B., Mistry, K., Murthy, A., Obradovic, B., Nagisetty, R., Nguyen, P., Sivakumar, S., Shaheed, R., Shifren, L., Tufts, B., Tyagi, S., Bohr, M., and El-Mansy, Y., 2004, "A 90-nm Logic Technology Featuring Strained-Silicon," IEEE Trans. Electron Devices, **51**(11), pp. 1790–1797.
[21] Pop, E., Dutton, R., and Goodson, K., 2005, "Monte Carlo Simulation of Joule Heating in Bulk and Strained Silicon," Appl. Phys. Lett., **86**, p. 082101.
[22] Mingo, N., and Yang, L., 2003, "Phonon Transport in Nanowires Coated With an Amorphous Material: An Atomistic Green's Function Approach," Phys. Rev. B, **68**, p. 245406.
[23] Mingo, N., and Yang, L., 2004, "Erratum: Phonon Transport in Nanowires Coated With an Amorphous Material: An Atomistic Green's Function Approach [Phys. Rev. B 68, 245406 (2003)]," Phys. Rev. B, **70**, p. 249901.
[24] Shilkrot, L., Srolovitz, D., and Tersoff, J., 2000, "Morphology Evolution During the Growth of Strained-Layer Superlattices," Phys. Rev. B, **62**(12), pp. 8397–8409.
[25] Ohring, M., 2001, *Materials Science of Thin Films*, Academic Press, New York, pp. 417–492.
[26] Wortman, J., and Evans, R., 1965, "Young's Modulus, Shear Modulus, and Poisson's Ratio in Silicon and Germanium," J. Appl. Phys., **36**, pp. 153–156.
[27] Harrison, W. A., 1989, *Electronic Structure and the Properties of Solids*, Dover, New York, pp. 181–208.
[28] Mingo, N., 2003, "Calculation of Si Nanowire Thermal Conductivity Using Complete Phonon Dispersion Relations," Phys. Rev. B, **68**, p. 113308.
[29] Keating, P. N., 1966, "Effect of Invariance Requirements on the Elastic Strain Energy of Crystals With Application to the Diamond Structure," Phys. Rev., **145**, pp. 637–645.
[30] Lannoo, M., and Friedel, P., 1991, *Atomic and Electronic Structure of Surfaces*, Springer, New York, pp. 42–48.
[31] Guinea, F., Tejedor, C., Flores, F., and Louis, E., 1983, "Effective Two-Dimensional Hamiltonian at Surfaces," Phys. Rev. B, **28**(8), pp. 4397–4402.
[32] Zhang, W., and Fisher, T., 2005, "Simulation of Phonon Interfacial Transport in Strained Silicon-Germanium Heterostructures," ASME Paper No. 80053.
[33] Datta, S., 2005, *Quantum Transport: Atom to Transistor*, 1st ed., Cambridge University Press, Cambridge, UK, pp. 223–233.
[34] Venugopal, R., Ren, Z., Datta, S., and Lundstrom, M., 2002, "Simulating Quantum Transport in Nanoscale Transistors: Real Versus Mode-Space Approaches," J. Appl. Phys., **92**, pp. 3730–3739.
[35] Kittel, C., 2005, *Introduction to Solid State Physics*, 8th ed., Wiley, New York, p. 108.
[36] Tascius, T., Liu, W., Liu, J., Zeng, T., Song, D., Moore, C., Chen, G., Wang, K., Goorsky, M., Radetic, T., Gronsky, R., Koga, T., and Dresselhaus, M., 2000, "Thermal Conductivity of Symmetrically Strained Si/Ge Superlattices," Superlattices Microstruct., **28**, pp. 199–206.
[37] Chakraborty, S., Kleint, C., Heinrich, A., Schneider, C., and Schumann, J., 2003, "Thermal Conductivity in Strain Symmetrized Si/Ge Superlattices on Si(111)," Appl. Phys. Lett., **83**, pp. 4184–4186.
[38] Lee, S.-M., Cahill, D., and Venkatasubramanian, R., 1997, "Thermal Conductivity of Si-Ge Superlattices," Appl. Phys. Lett., **70**, pp. 2957-2959.
[39] Stoner, R., and Maris, H., 1993, "Kapitza Conductance and Heat Flow Between Solids at Temperature From 50 to 300 K," Phys. Rev. B, **48**, pp. 16373–16387.
[40] Costescu, R., Wall, M., and Cahill, D., 2003, "Thermal Conductance of Epitaxial Interfaces," Phys. Rev. B, **67**, p. 054302.
[41] Cheeke, J., Ettinger, H., and Herbal, B., 1976, "Analysis of Heat Transfer Between Solids at Low Temperatures," Can. J. Phys., **54**, pp. 1749–1763.
[42] Holland, M., 1963, "Analysis of Lattice Thermal Conductivity," Phys. Rev., **132**, pp. 2461–2471.